

ORDER, DISORDER, AND PHASE TRANSITION  
IN CONDENSED SYSTEM

# Magnetic Properties of the $\text{Nd}_{0.95}\text{Dy}_{0.05}\text{Fe}_3(\text{BO}_3)_4$ Ferroborate with Small Substitution in the Rare-Earth Element Subsystem

A. I. Begunov<sup>a</sup>, A. A. Demidov<sup>a,\*</sup>, I. A. Gudim<sup>b</sup>, and E. V. Eremin<sup>b</sup>

<sup>a</sup> Bryansk State Technical University, Bryansk, 241035 Russia

\*e-mail: demandr@yandex.ru

<sup>b</sup> Kirensky Institute of Physics, Siberian Branch, Russian Academy of Sciences, Krasnoyarsk, 660038 Russia

Received January 12, 2013

**Abstract**—The magnetic properties of a substituted  $\text{Nd}_{0.95}\text{Dy}_{0.05}\text{Fe}_3(\text{BO}_3)_4$  ferroborate single crystal with competing Nd–Fe and Dy–Fe exchange interactions are studied experimentally and theoretically. A spontaneous spin-reorientation transition is detected near  $T = 4.3$  K, and anomalies are observed in the low-temperature magnetization curves along trigonal axis  $c$  and in basal plane  $ab$ . The measured properties and the detected effects are interpreted in terms of a general theoretical approach, which is based on the molecular field approximation and crystal field calculations for a rare-earth ion. The experimental temperature dependences of the initial magnetic susceptibility in the range 2–300 K, the anomalies in the magnetization curves for  $\mathbf{B} \parallel \mathbf{c}$  and  $\mathbf{B} \perp \mathbf{c}$  in fields up to 1.5 T, and the field and temperature dependences of magnetization in fields up to 9 T are described. The effect of small substitution in the rare-earth subsystem on the magnetic properties is analyzed. The crystal field parameters and the parameters of the R–Fe and Fe–Fe exchange interactions are determined from the experimental data.

DOI: 10.1134/S1063776113120108

## INTRODUCTION

Trigonal rare-earth  $\text{RFe}_3(\text{BO}_3)_4$  ( $\text{R} = \text{Y}, \text{La–Lu}$ ) ferroborates are being extensively studied by many research teams, which is explained by the discovery of multiferroelectric properties in them [1–7]. Antiferromagnetic ordering in the iron subsystem in the ferroborates occurs at  $T_N \approx 30–40$  K. The rare-earth subsystem is magnetized due to the  $f$ – $d$  interaction and significantly contributes to the magnetic anisotropy of the compound and the orientation of magnetic moments. The ferroborates were found to be easy-axis (magnetic moments of  $\text{R} = \text{Pr}, \text{Tb}, \text{Dy}, \text{Fe}$  are oriented along axis  $c$ ) and easy-plane (magnetic moments of  $\text{R} = \text{Y}, \text{Nd}, \text{Sm}, \text{Eu}, \text{Er}, \text{Fe}$  lie in plane  $ab$ ) ones or can spontaneously transform from an easy-axis into an easy-plane state (as in  $\text{GdFe}_3(\text{BO}_3)_4$  and  $\text{HoFe}_3(\text{BO}_3)_4$ ; see, e.g., review [4]).

Additional interest in the ferroborates is related to the recent possibility of studying substituted  $\text{R}_{1-x}\text{R}'_x\text{Fe}_3(\text{BO}_3)_4$  compositions, since new opportunities for varying a composition provide a larger variety of physical effects [3, 7–16]. The presence of competing R–Fe and R'–Fe exchange interactions in  $\text{R}_{1-x}\text{R}'_x\text{Fe}_3(\text{BO}_3)_4$  can result in the effects that are caused by the competition of contributions, e.g., spontaneous reorientation transitions between the easy-axis and easy-plane states [8, 10, 12–16].

The  $\text{Nd}^{3+}$  and  $\text{Dy}^{3+}$  ions are convenient rare-earth ions for forming and studying a substituted ferroborate

with competing exchange interactions. At  $T < T_N \approx 31$  K, the magnetic moments of the neodymium and iron subsystems in  $\text{NdFe}_3(\text{BO}_3)_4$  lie in the basal  $ab$  plane [2, 17]. The magnetic moments of Dy and Fe in the  $\text{DyFe}_3(\text{BO}_3)_4$  ferroborate at  $T < T_N \approx 39$  K are oriented along trigonal axis  $c$ , and this compound undergoes a spin-flop transition for  $\mathbf{B} \parallel \mathbf{c}$  [18]. The competition of the contributions of the  $\text{Nd}^{3+}$  and  $\text{Dy}^{3+}$  ions to the magnetic anisotropy of substituted ferroborates  $\text{Nd}_{1-x}\text{Dy}_x\text{Fe}_3(\text{BO}_3)_4$  can lead to spontaneous and magnetic field-induced spin-reorientation transitions from axis  $c$  to plane  $ab$ . In  $\text{Nd}_{0.75}\text{Dy}_{0.25}\text{Fe}_3(\text{BO}_3)_4$  [8, 10, 12] and  $\text{Nd}_{1-x}\text{Dy}_x\text{Fe}_3(\text{BO}_3)_4$  ( $x = 0.1, 0.15, 0.4$ ) [12–14], researchers detected anomalies in the behavior of magnetic susceptibility, magnetization, spontaneous electric polarization, magnetostriction, and magnetoacoustic characteristics and plotted  $H$ – $T$  diagrams for possible magnetic phases.

In particular, keen interest in  $\text{Nd}_{1-x}\text{Dy}_x\text{Fe}_3(\text{BO}_3)_4$  ferroborates is attracted by the existence of experimental data with a noncoincident number of anomalies in the magnetization curves of  $\text{Nd}_{0.75}\text{Dy}_{0.25}\text{Fe}_3(\text{BO}_3)_4$  for  $\mathbf{B} \parallel \mathbf{c}$  [8, 12]. Different opinions regarding the nature and mechanism of the anomalies were expressed, and different  $H$ – $T$  diagrams of possible magnetic phases appear [8, 10, 12, 16].

The purpose of this work is to experimentally and theoretically study the low-temperature magnetic properties of the weakly substituted  $\text{Nd}_{0.95}\text{Dy}_{0.05}\text{Fe}_3(\text{BO}_3)_4$  ferroborate, to compare the experimental data obtained in this work with the

results of calculations performed in terms of a general theoretical approach, and to determine the parameters of this compound.

## EXPERIMENTAL

Single crystals were grown from molten solutions based on bismuth trimolybdate, i.e., 75 wt % [Bi<sub>2</sub>Mo<sub>3</sub>O<sub>12</sub> + 3B<sub>2</sub>O<sub>3</sub> + 0.57Nd<sub>2</sub>O<sub>3</sub> + 0.03Dy<sub>2</sub>O<sub>3</sub>] + 25 wt % Nd<sub>0.95</sub>Dy<sub>0.05</sub>Fe<sub>3</sub>(BO<sub>3</sub>)<sub>4</sub>, in accordance with the technique described in detail in [19]. The crystals were 6–10 mm in size and had a small triangular {0001} pinacoid face normal to axis C<sub>3</sub>. The crystals had a good optical quality and did not contain visible defects. The neodymium and dysprosium concentrations in a crystal were determined by X-ray spectral fluorescent analysis. Magnetic measurements were performed on a Physical Properties Measurement System (Quantum Design) device in the temperature range 2–300 K and magnetic fields up to 9 T.

## COMPUTATION PROCEDURE

The magnetic properties of Nd<sub>1-x</sub>Dy<sub>x</sub>Fe<sub>3</sub>(BO<sub>3</sub>)<sub>4</sub> ferroborates are determined by both magnetic subsystems, i.e., the rare-earth (neodymium and dysprosium) subsystem and the iron subsystem, which interact with each other. The interaction within the R subsystem can be neglected, and the iron subsystem can be considered as a set of two antiferromagnetic sublattices. The R subsystem magnetized due to the *f-d* interaction can also be represented in the form of two sublattices.

In our calculations, we used the theoretical approach that was successfully employed for RFe<sub>3</sub>(BO<sub>3</sub>)<sub>4</sub> ferroborates with R = Tb [20], Nd [17], Dy [18], Pr [21], Ho [22], and Er [23] and for ferroborates with substituted compositions Nd<sub>1-x</sub>Dy<sub>x</sub>Fe<sub>3</sub>(BO<sub>3</sub>)<sub>4</sub> (*x* = 0.1, 0.15, 0.25, 0.4) [12–14] and Tb<sub>0.25</sub>Er<sub>0.75</sub>Fe<sub>3</sub>(BO<sub>3</sub>)<sub>4</sub> [23]. This theoretical approach is based on a crystal field model for the R subsystem and the molecular field approximation.

Based on the magnetic structure and the hierarchy of interactions in Nd<sub>1-x</sub>Dy<sub>x</sub>Fe<sub>3</sub>(BO<sub>3</sub>)<sub>4</sub>, we can write the effective Hamiltonians of an R/Fe ion of the *i*th (*i* = 1, 2) sublattice in magnetic field **B** in the form

$$\mathcal{H}_i(\text{R}) = \mathcal{H}_i^{\text{CF}} - g_J^{\text{R}} \mu_B \mathbf{J}_i^{\text{R}} [\mathbf{B} + \lambda_{\text{fd}}^{\text{R}} \mathbf{M}_i^{\text{Fe}}], \quad (1)$$

$$\begin{aligned} \mathcal{H}_i(\text{Fe}) &= -g_S \mu_B \mathbf{S}_i \\ &\times [\mathbf{B} + \lambda \mathbf{M}_j^{\text{Fe}} + (1-x)\lambda_{\text{fd}}^{\text{Nd}} \mathbf{m}_i^{\text{Nd}} + x\lambda_{\text{fd}}^{\text{Dy}} \mathbf{m}_i^{\text{Dy}}], \quad (2) \\ &j = 1, 2, \quad j \neq i. \end{aligned}$$

Here,  $\mathcal{H}_i^{\text{CF}}$  is the crystal field Hamiltonian,  $g_J^{\text{R}}$  is the Lande factor,  $\mathbf{J}_i^{\text{R}}$  is the angular momentum operator of the R ion,  $g_S = 2$  is the *g* factor,  $\mathbf{S}_i$  is the spin moment operator of the iron ion, and  $\lambda_{\text{fd}}^{\text{R}} < 0$  and  $\lambda < 0$  are the

molecular constants of the antiferromagnetic R–Fe and Fe–Fe interactions.

The magnetic moments of the *i*th iron ( $\mathbf{M}_i^{\text{Fe}}$ ) and rare-earth ( $\mathbf{m}_i^{\text{R}}$ ) sublattices per formula unit are determined by the relationships

$$\mathbf{M}_i^{\text{Fe}} = 3g_S \mu_B \langle \mathbf{S}_i \rangle, \quad \mathbf{m}_i^{\text{R}} = g_J^{\text{R}} \mu_B \langle \mathbf{J}_i^{\text{R}} \rangle. \quad (3)$$

The Fe<sup>3+</sup> ion in RFe<sub>3</sub>(BO<sub>3</sub>)<sub>4</sub> is in a high-spin state [24], which causes the maximum magnetic moment of the ion (5μ<sub>B</sub>).

An expression for crystal field Hamiltonian  $\mathcal{H}^{\text{CF}}$  in terms of irreducible tensor operators  $C_q^k$  has the form

$$\begin{aligned} \mathcal{H}^{\text{CF}} &= B_0^2 C_0^2 + B_0^4 C_0^4 + B_3^4 (C_{-3}^4 - C_3^4) + B_0^6 C_0^6 \\ &+ B_3^6 (C_{-3}^6 - C_3^6) + B_6^6 (C_{-6}^6 + C_6^6). \quad (4) \end{aligned}$$

Crystal field parameters  $B_q^k$  for the Nd<sup>3+</sup> and Dy<sup>3+</sup> ions in Nd<sub>0.95</sub>Dy<sub>0.05</sub>Fe<sub>3</sub>(BO<sub>3</sub>)<sub>4</sub> are unknown. Certain information concerning the splitting of the ground multiplet of the Nd<sup>3+</sup> and Dy<sup>3+</sup> ions in Nd<sub>0.95</sub>Dy<sub>0.05</sub>Fe<sub>3</sub>(BO<sub>3</sub>)<sub>4</sub> is also unavailable. With allowance for the small degree of substitution of Dy<sup>3+</sup> for Nd<sup>3+</sup> ions in Nd<sub>0.95</sub>Dy<sub>0.05</sub>Fe<sub>3</sub>(BO<sub>3</sub>)<sub>4</sub>, it is helpful to use data on the structure of the ground multiplet of the Nd<sup>3+</sup> ion in the NdFe<sub>3</sub>(BO<sub>3</sub>)<sub>4</sub> ferroborate for calculations. It is known from the spectroscopic studies in [25] that the splitting of the ground doublet of the Nd<sup>3+</sup> ion in NdFe<sub>3</sub>(BO<sub>3</sub>)<sub>4</sub> is Δ<sub>fd</sub> = 8.8 cm<sup>-1</sup>. Using the data on Δ<sub>fd</sub> and the comprehensive experimental data on the magnetic properties of NdFe<sub>3</sub>(BO<sub>3</sub>)<sub>4</sub> from [17], we calculated the structure of the ground multiplet of the Nd<sup>3+</sup> ion; it is characterized by energies of 0, 8.8, 69, 69, 140, and 148 cm<sup>-1</sup> at *T* = 2 K.

The computation of the values and orientations of the magnetic moments of the Fe and R subsystems in solving the self-consistent problems using Hamiltonians (1) and (2) at the minimum of the corresponding thermodynamic potential makes it possible to calculate the stability regions of various magnetic phases, the phase-transition fields, magnetization curves, the susceptibility, and so on. In terms of the standard thermodynamic perturbation theory described in monograph [26] for *f-d* compounds, the corresponding thermodynamic potential can be written as

$$\begin{aligned} \Phi(T, B) &= \frac{1}{2} \sum_{i=1}^2 \left[ -(1-x)k_B T \ln Z_i(\text{Nd}) \right. \\ &- xk_B T \ln Z_i(\text{Dy}) + (1-x) \frac{1}{2} g_J^{\text{Nd}} \mu_B \langle \mathbf{J}_i^{\text{Nd}} \rangle \lambda_{\text{fd}}^{\text{Nd}} \mathbf{M}_i^{\text{Fe}} \\ &+ x \frac{1}{2} g_J^{\text{Dy}} \mu_B \langle \mathbf{J}_i^{\text{Dy}} \rangle \lambda_{\text{fd}}^{\text{Dy}} \mathbf{M}_i^{\text{Fe}} - 3k_B T \ln Z_i(\text{Fe}) \quad (5) \\ &+ \left. \frac{1}{2} 3g_S \mu_B \langle \mathbf{S}_i \rangle (\lambda \mathbf{M}_j^{\text{Fe}} + (1-x)\lambda_{\text{fd}}^{\text{Nd}} \mathbf{m}_i^{\text{Nd}} \right) \end{aligned}$$

$$+ x\lambda_{\text{fd}}^{\text{Dy}} \mathbf{m}_i^{\text{Dy}}) + \Phi_{\text{an}}^i \Big],$$

where  $Z_i(\text{R/Fe})$  are the partition functions calculated with Hamiltonians (1) and (2) and  $\Phi_{\text{an}}^i$  is the anisotropy energy for the  $i$ th sublattice of the Fe system. For a crystal of trigonal symmetry (see. e.g., [27]), this energy is

$$\begin{aligned} \Phi_{\text{an}}^i &= K_2^{\text{Fe}} \sin^2 \vartheta_i + K_4^{\text{Fe}} \sin^4 \vartheta_i \\ &+ K_{66}^{\text{Fe}} \sin^6 \vartheta_i \cos 6\varphi_i, \end{aligned} \quad (6)$$

where anisotropy constant  $K_2^{\text{Fe}} < 0$  stabilizes the easy-plane antiferromagnetic state; constant  $K_4^{\text{Fe}} > 0$  stabilizes the easy-axis state;  $K_{66}^{\text{Fe}} < 0$  is the anisotropy constant in the basal  $ab$  plane; and  $\vartheta_i$  and  $\varphi_i$  are the polar and azimuth angles of magnetic moment vector  $\mathbf{M}_i^{\text{Fe}}$  of iron, respectively.

Three types of domains can exist in a trigonal crystal with magnetic moments lying in the basal plane. The magnetization of  $\text{Nd}_{1-x}\text{Dy}_x\text{Fe}_3(\text{BO}_3)_4$  (per formula unit with allowance for possible existence of three types of domains;  $n = 1, 2, 3$ ) is

$$\mathbf{M} = \frac{1}{3} \sum_{n=1}^3 \frac{1}{2} \sum_{i=1}^2 (\mathbf{M}_i^{\text{Fe}} + (1-x)\mathbf{m}_i^{\text{Nd}} + x\mathbf{m}_i^{\text{Dy}}). \quad (7)$$

The rare-earth and iron subsystems contribute to the magnetic susceptibility of  $\text{Nd}_{1-x}\text{Dy}_x\text{Fe}_3(\text{BO}_3)_4$  as follows:

$$\chi_k = \chi_k^{\text{Fe}} + (1-x)\chi_k^{\text{Nd}} + x\chi_k^{\text{Dy}}, \quad k = a, b, c. \quad (8)$$

In the ordered phase, the initial magnetic susceptibilities of the compound can be found from the initial linear segments of the magnetization curves calculated for the corresponding directions of an external magnetic field. In the paramagnetic region (where the interaction between the R and Fe subsystems can be neglected), the magnetic susceptibility of the R subsystem can be calculated using the well-known Van Vleck formula, the energy spectrum and wavefunctions for which are calculated using crystal field Hamiltonian (4). Susceptibility  $\chi_p^{\text{Fe}}$  of the Fe subsystem can be described by the Curie–Weiss law with the corresponding paramagnetic Néel temperature  $\Theta$ ,

$$\begin{aligned} \chi_p^{\text{Fe}} &= \frac{\mu_{\text{eff}}^2}{3k_B(T - \Theta)}, \\ \mu_{\text{eff}}^2 &= 105\mu_B^2 \text{ for } S = \frac{5}{2}. \end{aligned} \quad (9)$$

## RESULTS AND DISCUSSION

To determine parameters  $B_q^k$  of the crystal field (which forms the electronic structure of a rare-earth

ion), we used the experimental data for the temperature dependences of initial magnetic susceptibility  $\chi_{c,\perp c}(T)$ . As the initial values of parameters  $B_q^k$ , we took the parameters for ferrobamate  $\text{NdFe}_3(\text{BO}_3)_4$  studied earlier [17] and for substituted ferrobamate  $\text{Nd}_{0.9}\text{Dy}_{0.1}\text{Fe}_3(\text{BO}_3)_4$  [13]. To determine which of the found sets of  $B_q^k$  parameters can describe the entire set of the measured magnetic characteristics of  $\text{Nd}_{0.95}\text{Dy}_{0.05}\text{Fe}_3(\text{BO}_3)_4$ , we calculated magnetization curves along the trigonal axis and in the basal plane ( $M_{c,\perp c}(B)$ ) at  $T = 2$  K to choose parameters  $\lambda_{\text{fd}}^{\text{R}}$  (antiferromagnetic Nd–Fe and Dy–Fe interactions) and  $\lambda_1$  (intrachain antiferromagnetic Fe–Fe interaction).

Another important criterion for the final choice of the crystal field parameters is to describe the spontaneous spin-reorientation transition temperature detected in  $\text{Nd}_{0.95}\text{Dy}_{0.05}\text{Fe}_3(\text{BO}_3)_4$  ( $T_{\text{SR}} \approx 4.3$  K; see below). Our calculations show that this criterion imposes substantial restrictions on parameters  $B_q^k$ .

Thus, following these criteria of describing the  $\chi_{c,\perp c}(T)$  and  $M_{c,\perp c}(B)$  curves and temperature  $T_{\text{SR}}$ , we chose the following set among the crystal field parameters found at the initial stage that ensures the best description of the experimental data for  $\text{Nd}_{0.95}\text{Dy}_{0.05}\text{Fe}_3(\text{BO}_3)_4$ :

$$\begin{aligned} B_0^2 &= 597 \text{ cm}^{-1}, & B_0^4 &= -1400 \text{ cm}^{-1}, \\ B_3^4 &= -370 \text{ cm}^{-1}, & B_0^6 &= 470 \text{ cm}^{-1}, \\ B_3^6 &= -490 \text{ cm}^{-1}, & B_6^6 &= 390 \text{ cm}^{-1}. \end{aligned} \quad (10)$$

These parameters were determined in the calculations based on the ground multiplet; therefore, they can only be treated as effective parameters suitable for describing the thermodynamic properties of the compound.

The set of parameters (10) corresponds to the energies of the lower levels of the ground multiplet of the  $\text{Nd}^{3+}$  and  $\text{Dy}^{3+}$  ions in  $\text{Nd}_{0.95}\text{Dy}_{0.05}\text{Fe}_3(\text{BO}_3)_4$  that are given in Table 1 for  $B = 0$ . These energies are given for  $T > T_{\text{N}}$  with allowance for the  $f$ – $d$  interaction at  $T = 5$  K  $> T_{\text{SR}}$  (easy-plane state) and  $T = 2$  K  $< T_{\text{SR}}$  (initial state, see below). Taking into account the  $f$ – $d$  interaction at  $T < T_{\text{N}}$  removes the degeneracy of the lower levels. At  $T_{\text{SR}}$ , the energy levels shift with respect to each other: in the case of Dy, the shift of the lower energy levels increases the splitting from  $\Delta_{\text{fd}} \approx 1.9$  to  $5.2$   $\text{cm}^{-1}$ ; in the case of Nd, this shift causes a small narrowing from  $\Delta_{\text{fd}} \approx 10.1$  to  $9.9$   $\text{cm}^{-1}$ . Note that the energies of the lower levels of the ground multiplet of the  $\text{Nd}^{3+}$  ion in  $\text{Nd}_{0.95}\text{Dy}_{0.05}\text{Fe}_3(\text{BO}_3)_4$  at  $T = 2$  K agree with those found for the  $\text{Nd}^{3+}$  ion in  $\text{NdFe}_3(\text{BO}_3)_4$  in [17] ( $\Delta = 0, 8.8, 69, 69, 140, 148$   $\text{cm}^{-1}$ ).

The calculated magnetic characteristics presented below in the figures were calculated for the parameters given in Table 2, which also gives the parameters of

Nd<sub>1-x</sub>Dy<sub>x</sub>Fe<sub>3</sub>(BO<sub>3</sub>)<sub>4</sub> ( $x = 0.1, 0.15, 0.25, 0.4$ ) [12–14] and ferrobates NdFe<sub>3</sub>(BO<sub>3</sub>)<sub>4</sub> [17] and DyFe<sub>3</sub>(BO<sub>3</sub>)<sub>4</sub> [18] for comparison. Parameter  $\lambda_2$  in Table 2 enters into the Brillouin function, is responsible for the magnetic moment of Fe (at given  $T$  and  $B$ ), and determines the Néel temperature, since the three-dimensional order in the structure of a ferrobate cannot exist without the exchange interaction between Fe<sup>3+</sup> ion chains. The value of parameter  $\lambda_2$  was chosen from the condition of the best agreement between the calculated and experimental  $M_{c,\perp c}(B)$  curves at all temperatures. In the calculations, we also use the uniaxial anisotropy constants of iron ( $K_2^{\text{Fe}} = -6.075 \text{ T } \mu_{\text{B}}$ ,  $K_4^{\text{Fe}} = 3.925 \text{ T } \mu_{\text{B}}$  at  $T = 4.2 \text{ K}$ ) and the anisotropy constant of iron in the basal plane ( $K_{66}^{\text{Fe}} = -1.35 \times 10^{-2} \text{ T } \mu_{\text{B}}$ ) [17]. When determining constants  $K^{\text{Fe}}$ , we took into account that the resulting anisotropy field of the Fe subsystem (see Eq. (6)) is  $-2.163 \text{ T } \mu_{\text{B}}$  at  $\theta = 90^\circ$ , which corresponds to  $-1.44 \text{ kOe}$  for the Fe subsystem in YbFe<sub>3</sub>(BO<sub>3</sub>)<sub>4</sub> [28]. Note that it was sufficient to take into account only one uniaxial constant  $K_2^{\text{Fe}}$  to describe the entire set of the experimental characteristics of Nd<sub>1-x</sub>Dy<sub>x</sub>Fe<sub>3</sub>(BO<sub>3</sub>)<sub>4</sub> ( $x = 0.1, 0.15, 0.25, 0.4$ ) in [12–14]. The introduction of a second constant ( $K_4^{\text{Fe}}$ ) for the case of Nd<sub>0.95</sub>Dy<sub>0.05</sub>Fe<sub>3</sub>(BO<sub>3</sub>)<sub>4</sub> is caused by the formation of a canted phase, which is necessary for a quantitative description of the measured characteristics (see below).

It is seen from Table 2 that constants  $\lambda_{\text{fd}}^{\text{R}}$  and exchange fields  $B_{\text{fd}}^{\text{R}} = |\lambda_{\text{fd}}^{\text{R}}| M_0$  of Nd<sub>1-x</sub>Dy<sub>x</sub>Fe<sub>3</sub>(BO<sub>3</sub>)<sub>4</sub> ( $x = 0.05-0.4$ ) differ from  $\lambda_{\text{fd}}^{\text{R}}$  and  $B_{\text{fd}}^{\text{R}}$  in NdFe<sub>3</sub>(BO<sub>3</sub>)<sub>4</sub> and DyFe<sub>3</sub>(BO<sub>3</sub>)<sub>4</sub>. For the Nd subsystem, exchange field  $B_{\text{fd}}^{\text{Nd}} = |\lambda_{\text{fd}}^{\text{Nd}}| M_0 = \Delta_{\text{fd}}^{\text{Nd}} / \mu_{\text{B}} g_{c,\perp c}$  in the easy-axis state ( $x = 0.1-0.4$ ) at  $g_c < g_{\perp c}$  and similar values of  $\Delta_{\text{fd}}^{\text{Nd}}$  is higher than in the easy-plane state ( $x = 0$ ). Note that the exchange field of the R ion in easy-axis PrFe<sub>3</sub>(BO<sub>3</sub>)<sub>4</sub>, which is close to NdFe<sub>3</sub>(BO<sub>3</sub>)<sub>4</sub>, is  $B_{\text{fd}}^{\text{Pr}} = 11 \text{ T}$  [21], which agrees with the field ( $B_{\text{fd}}^{\text{Nd}} = 11.5-13.5 \text{ T}$ ) found for Nd<sub>1-x</sub>Dy<sub>x</sub>Fe<sub>3</sub>(BO<sub>3</sub>)<sub>4</sub> ( $x = 0.1-0.4$ ) in the easy-axis state. The decrease of  $B_{\text{fd}}^{\text{R}}$  and  $\lambda_{\text{fd}}^{\text{R}}$  with decreasing  $x$  (for  $x = 0.1-0.4$ ) that is seen in Table 2 is related to the anomalies in the experimental  $M_c(B)$  curves when spin-flop transition field  $B_{\text{SR}}$  decreases, since the antiparallel orientation of vectors  $m_{1c}^{\text{Dy}_x}$  and  $m_{2c}^{\text{Dy}_x}$  in the easy-axis state at  $T \leq 4.2 \text{ K}$  causes a high sensitivity of the initial segment of the  $M_c(B)$  magnetization curve (at  $B < B_{\text{SR}}$ ) to parameters  $B_{\text{fd}}^{\text{Dy}}$  and  $\lambda_{\text{fd}}^{\text{Dy}}$ .

**Table 1.** Energies of the eight lower levels of the ground multiplets of the Nd<sup>3+</sup> and Dy<sup>3+</sup> ions in Nd<sub>0.95</sub>Dy<sub>0.05</sub>Fe<sub>3</sub>(BO<sub>3</sub>)<sub>4</sub> at  $B = 0$  that are split by the crystal field (parameters (10)) in the paramagnetic and ordered (with allowance for the  $f$ - $d$  interaction) temperature ranges

$R$	$T$	$\Delta = E_i - E^1, \text{ cm}^{-1} (i = 1-8)$
Nd	$T > T_{\text{N}}$	0, 0, 55.1, 55.1, 155, 155, 286, 286
	5 K $> T_{\text{SR}}$	0, 10.1, 60.7, 60.8, 156, 165, 291, 291
	2 K $< T_{\text{SR}}$	0, 9.9, 58.9, 62.5, 155.6, 165, 289, 292
Dy	$T > T_{\text{N}}$	0, 0, 13.3, 13.3, 104.8, 104.8, 222, 222
	5 K $> T_{\text{SR}}$	0, 1.9, 15.9, 17.8, 107.3, 107.3, 222, 226
	2 K $< T_{\text{SR}}$	0, 5.2, 16.2, 20.7, 107.2, 110.6, 223, 228

To calculate the magnetic characteristics of Nd<sub>0.95</sub>Dy<sub>0.05</sub>Fe<sub>3</sub>(BO<sub>3</sub>)<sub>4</sub> when an external field is directed along or perpendicular to trigonal axis  $c$ , we used the schemes of orientation of the magnetic moments of iron  $\mathbf{M}_i^{\text{Fe}}$  and a rare-earth element  $\mathbf{m}_i^{\text{R}}$  shown in Fig. 1. The calculations according to the schemes in Figs. 1a and 1d were performed for a field directed along the trigonal axis ( $\mathbf{B} \parallel \mathbf{c}$ ). The schemes in Figs. 1b and 1d were used for the case of a magnetic field oriented in the basal plane ( $\mathbf{B} \perp \mathbf{c}$ ), and the scheme in Fig. 1c is shown for the case of  $B = 0$  (cone of easy magnetization axes). The scheme in Fig. 1c shows the projections of the magnetic moments of the iron ( $\mathbf{M}_{\text{iab}}^{\text{Fe}}$ ) and rare-earth ( $\mathbf{m}_{\text{iab}} = (1-x)\mathbf{m}_{\text{iab}}^{\text{Nd}} + x\mathbf{m}_{\text{iab}}^{\text{Dy}}$ ) subsystems onto the  $ab$  plane in domains with antiferromagnetism axes making angles  $\varphi_i = 0 (L_0)$  and  $60^\circ (L_{60})$  with the  $a$  axis.

At  $B > 1.5 \text{ T}$ , NdFe<sub>3</sub>(BO<sub>3</sub>)<sub>4</sub> is known to be in the flop phase and to behave like a single-domain compound, and the magnetic moments of the Fe and Nd subsystems are located in basal plane  $ab$  [17]. Then, taking into account the small substitution of Dy<sup>3+</sup> for Nd<sup>3+</sup> ions, we first consider the magnetic properties of Nd<sub>0.95</sub>Dy<sub>0.05</sub>Fe<sub>3</sub>(BO<sub>3</sub>)<sub>4</sub> at  $B > 1.5 \text{ T}$  by assuming that its magnetic subsystem in this field range exhibits easy-plane properties (scheme in Fig. 1a for  $\mathbf{B} \parallel \mathbf{c}$  and scheme in Fig. 1b for  $\mathbf{B} \perp \mathbf{c}$ ). In this state, the magnetic moments of the Fe sublattices ( $\mathbf{M}_1^{\text{Fe}}, \mathbf{M}_2^{\text{Fe}}$ ) bend toward the field direction and exhibit perpendicular susceptibility, which is temperature independent for a typical antiferromagnet, and the component of the magnetic moment onto the field direction in the  $R$  subsystem increases.

It is seen from the experimental and calculated  $M_{c,\perp c}(B)$  magnetization curves of Nd<sub>0.95</sub>Dy<sub>0.05</sub>Fe<sub>3</sub>(BO<sub>3</sub>)<sub>4</sub> at  $T = 2 \text{ K}$  that the  $M_c(B)$  and  $M_{\perp c}(B)$  curves increase monotonically at different rates with the field at  $B > 1.5 \text{ T}$  (see Fig. 2). A comparison of the contributions of the Nd, Dy, and Fe subsystems to the magne-

**Table 2.** Parameters of  $\text{Nd}_{0.95}\text{Dy}_{0.05}\text{Fe}_3(\text{BO}_3)_4$ ,  $\text{Nd}_{1-x}\text{Dy}_x\text{Fe}_3(\text{BO}_3)_4$  ( $x = 0.1, 0.15, 0.25, 0.4$ ) [12–14],  $\text{NdFe}_3(\text{BO}_3)_4$  [17], and  $\text{DyFe}_3(\text{BO}_3)_4$  [18]

Compound		NdFe	$\text{Nd}_{1-x}\text{Dy}_x\text{Fe}_3(\text{BO}_3)_4$					DyFe
			$x = 0.05$	$x = 0.1$	$x = 0.15$	$x = 0.25$	$x = 0.4$	
$B_{dd1} = \lambda_1 M_0$ , T		58	62	56	54	54	52	53
$\lambda_1$ , T/ $\mu_B$		-3.87	-4.13	-3.73	-3.6	-3.6	-3.47	-3.53
$B_{dd2} = \lambda_2 M_0$ , T		27	32.5	31	30	28.5	27.5	28
$\lambda_2$ , T/ $\mu_B$		-1.8	-2.17	-2.1	-2	-1.9	-1.83	-1.87
$B_{fd} = \lambda_{fd}^R M_0$ , T	Nd	7.1	8.32	12.7	11.5	11.5	13.5	
	Dy		2.84	1.1	2	2.3	2.5	3.3
$\lambda_{fd}^R$ , T/ $\mu_B$	Nd	-0.47	-0.55	-0.85	-0.77	-0.77	-0.9	
	Dy		-0.19	-0.07	-0.13	-0.15	-0.17	-0.22
$\Delta_{fd}$ , $\text{cm}^{-1}$	Nd	EA		~8.8	~8	~8.2	~6.8	
		EP	~8.8	~10.1	~14.6	~13	~16	
		CEMA		~9.9				
	Dy	EA			~8.2	~15.7	~17.8	~19.2
EP			~1.9	~0.6	~0.8	~0.9	~1	
CEMA			~5.2					
$B_{SR}$ , T	$\mathbf{B} \parallel \mathbf{c}$		~0.35	~0.84	0.9*, 1.1, 1.26	1.46*, 1.66	1.9	2.8
	$\mathbf{B} \perp \mathbf{c}$	0.7–0.8	~0.9					
$\vartheta_1$ , deg ( $B = 0$ )		90	~77	→ 0?	→ 0?	→ 0	0	0
$T_{SR}$ , K			~4.3	~8	~12.5	~16, 24*	~31	
$T_N$ , K		~31	~30	~31	~31	~31	~32	~39
$\Theta$ , K		-130	-135	-131	-132	-135	-135	-180

Note:  $B_{dd1}$  (intrachain Fe–Fe),  $B_{dd2}$  (interchain Fe–Fe), and  $B_{fd}$  are the low-temperature exchange fields corresponding to molecular constants  $\lambda_1$ ,  $\lambda_2$ , and  $\lambda_{fd}^R$ , respectively.  $\Delta_{fd} = \mu_B g |\lambda_{fd}^R| M_0$  is the low-temperature splitting of the ground state of an  $R$  ion due to the  $f$ – $d$  interaction in the following states: a cone of easy magnetization axes (CEMA), easy-axis (EA) state, and easy-plane (EP) state.  $\vartheta_1$  is the angle of deviation of  $\mathbf{M}_0^{\text{Fe}}$  from axis  $c$ .  $T_{SR}$  is the spin-reorientation transition temperature.  $T_N$  is the Néel temperature.  $\Theta$  is the paramagnetic Néel temperature for the Fe subsystem.  $M_0 = |M_f(T = 0, B = 0)| = 15 \mu_B$  is the magnetic moment of iron per formula unit. Steplike anomalies in the  $M_c(B)$  and  $\chi_c(T)$  curves are observed at  $x = 0.15$  and  $0.25$  (marked by asterisk) [12].

tization of  $\text{Nd}_{0.95}\text{Dy}_{0.05}\text{Fe}_3(\text{BO}_3)_4$  that were calculated in the flop phase for  $\mathbf{B} \parallel \mathbf{c}$ ,  $\mathbf{B} \perp \mathbf{c}$  demonstrates the difference in their behavior, which explains the detected different rates of increase of the experimental  $M_{\perp c}(B)$  curves with the field. The contributions of the Dy and Nd subsystems for  $\mathbf{B} \parallel \mathbf{c}$ ,  $\mathbf{B} \perp \mathbf{c}$  differ substantially, and the contribution of the Fe subsystem weakly depends on the field direction.

We also show the experimental and calculated magnetization curves in fields up to 9 T along the trigonal axis (Fig. 3,  $M_{\perp c}(B)$ ) and in the basal plane (Fig. 4,  $M_{c, \perp c}(B)$ ) in the temperature range  $T = 2$ –40 K. As the temperature increases, the  $M_{\perp c}(B)$  curves become less sharp and the magnetization curves evolve due to a decrease in the magnetic moments of the R and Fe subsystems. As is seen from Figs. 2–4, the calculations on the assumption of an easy-plane state of

the magnetic subsystem in  $\text{Nd}_{0.95}\text{Dy}_{0.05}\text{Fe}_3(\text{BO}_3)_4$  well describe the behavior of the experimental  $M_{c, \perp c}(B)$  curves for  $B > 1.5$  T at  $T = 2$  K and over the entire field range at  $T = 10, 20$ , and 40 K. Figures 3 and 4 also show the calculated contributions of the Nd, Dy, and Fe subsystems to the magnetization of the compound at  $T = 10$  K, and a comparison of these contributions demonstrates the responsibility of each contribution for the resulting shape of the  $M_{c, \perp c}(B)$  curves.

In low fields ( $B < 1.5$  T), the experimental  $M_{c, \perp c}(B)$  magnetization curves recorded at  $T = 2$  K exhibit a pronounced anomaly in the  $M_c(B)$  curve near 0.35 T and a smooth jump in the  $M_{\perp c}(B)$  curve near 0.9 T, which point to a substantial change in the contributions of the R and Fe subsystems to the magnetization of the compound during magnetization both along axis  $c$  and in basal plane  $ab$  (see Fig. 2).

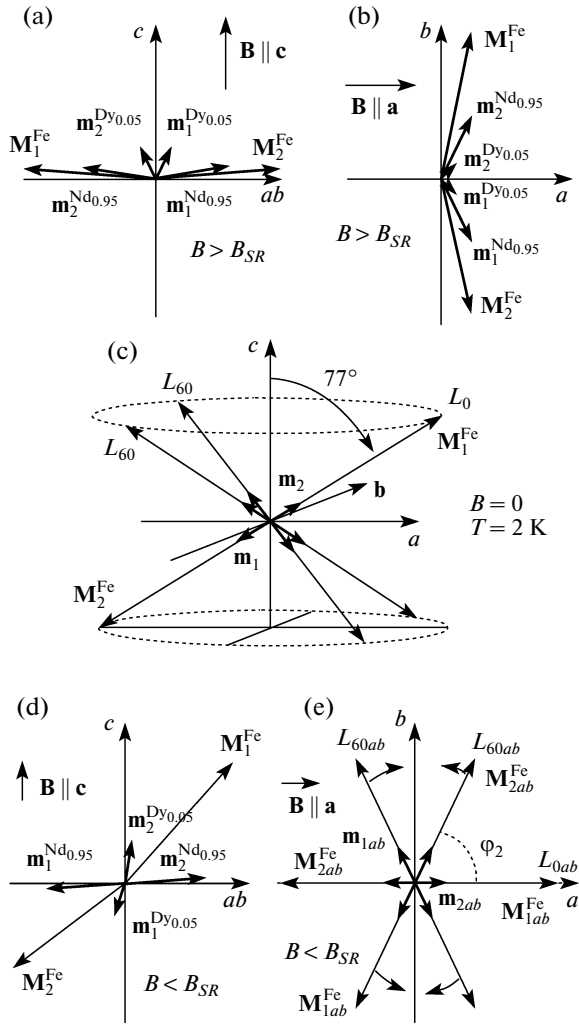


**Fig. 1.** Schematic diagrams for the orientations of the magnetic moments of iron ( $M_i^{\text{Fe}}$ ) and a rare-earth element ( $m_i^{\text{R}}$ ) used to calculate the magnetic properties of  $\text{Nd}_{0.95}\text{Dy}_{0.05}\text{Fe}_3(\text{BO}_3)_4$  for various magnetic field directions: (a), (d)  $\mathbf{B} \parallel \mathbf{c}$  (plane  $ab$  is perpendicular to the figure plane); (b), (e)  $\mathbf{B} \perp \mathbf{c}$  (axis  $c$  is perpendicular to the figure plane); and (c)  $B = 0$  (cone of easy magnetization axes).

Let us dwell on the low-field region of the experimental  $M_{c,\perp c}(B)$  magnetization curves at  $T = 2$  K, which is separately shown in Fig. 5 (the curves in Fig. 2 are presented in fields up to 9 T). For comparison, Fig. 5 also shows the experimental  $M_{c,a}^{\text{NdFe}}(B)$  curves of the  $\text{NdFe}_3(\text{BO}_3)_4$  ferroborate [29]. It is seen that small ( $x = 0.05$ ) substitution of  $\text{Dy}^{3+}$  for  $\text{Nd}^{3+}$  ions only weakly affects the magnetization in the basal plane: the  $M_{\perp c}(B)$  curve of  $\text{Nd}_{0.95}\text{Dy}_{0.05}\text{Fe}_3(\text{BO}_3)_4$  repeats the shape of  $M_a^{\text{NdFe}}(B)$  of  $\text{NdFe}_3(\text{BO}_3)_4$  and lies slightly higher. However, this small substitution radically changes the shape of the  $M_c(B)$  curve of

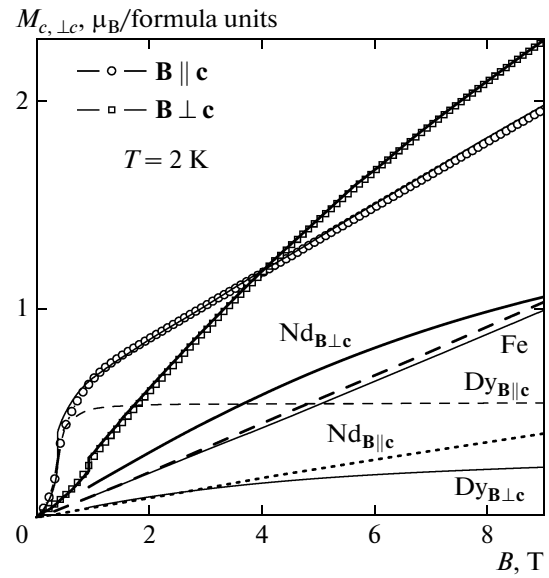


**Fig. 2.** Magnetization curves of  $\text{Nd}_{0.95}\text{Dy}_{0.05}\text{Fe}_3(\text{BO}_3)_4$  for  $\mathbf{B} \parallel \mathbf{c}$  and  $\mathbf{B} \perp \mathbf{c}$  at  $T = 2$  K: (symbols) experimental data and (curves) calculation. Calculated contributions of the Nd, Dy, and Fe subsystems to the total magnetization in the flop phase for (dashed curves)  $\mathbf{B} \parallel \mathbf{c}$  and (solid curves)  $\mathbf{B} \perp \mathbf{c}$ .

$\text{Nd}_{0.95}\text{Dy}_{0.05}\text{Fe}_3(\text{BO}_3)_4$ . The appearing contribution of the  $\text{Dy}_{0.05}$  subsystem significantly changes magnetization  $M_c(B)$  and causes a pronounced anomaly near 0.35 T, which is absent in  $M_c^{\text{NdFe}}(B)$ .

If the  $M_{c,\perp c}(B)$  curves of  $\text{Nd}_{0.95}\text{Dy}_{0.05}\text{Fe}_3(\text{BO}_3)_4$  at  $T = 2$  K are differentiated, the curves of differential magnetic susceptibility  $dM_{c,\perp c}/dB(B)$  exhibit pronounced peaks at 0.35 T (for  $\mathbf{B} \parallel \mathbf{c}$ ) and 0.9 T (for  $\mathbf{B} \perp \mathbf{c}$ ). Note that the character of the low-temperature magnetic state of the weakly substituted  $\text{Nd}_{0.95}\text{Dy}_{0.05}\text{Fe}_3(\text{BO}_3)_4$  ferroborate is unknown and that its determination and the subsequent description of the detected anomalies in  $M_c(B)$  and  $M_{\perp c}(B)$ , which indicate phase transitions from the initial into the easy-plane state, are not obvious.

In [12–14], we showed for  $\text{Nd}_{1-x}\text{Dy}_x\text{Fe}_3(\text{BO}_3)_4$  ( $x = 0.1, 0.15, 0.25, 0.4$ ) ferroborates that the magnetic moments of the Nd, Dy, and Fe subsystems at low temperatures and  $B = 0$  are oriented along trigonal axis  $c$ . However, the experimental magnetization curves of  $\text{Nd}_{1-x}\text{Dy}_x\text{Fe}_3(\text{BO}_3)_4$  ( $x = 0.1, 0.15, 0.25, 0.4$ ) exhibited anomalies only in the  $M_c(B)$  curve, and the  $M_{\perp c}(B)$  curves increased monotonically with the field without visible anomalies even at  $T = 2$  K [12–14]. The magnetization curves of the easy-axis  $\text{DyFe}_3(\text{BO}_3)_4$  ferroborate also have pronounced specific features only for one direction of an applied field, namely, along trigonal axis  $c$  [18].

We could assume that the ground low-temperature magnetic state in  $\text{Nd}_{0.95}\text{Dy}_{0.05}\text{Fe}_3(\text{BO}_3)_4$  is the same as in easy-plane  $\text{NdFe}_3(\text{BO}_3)_4$  because of small substitu-

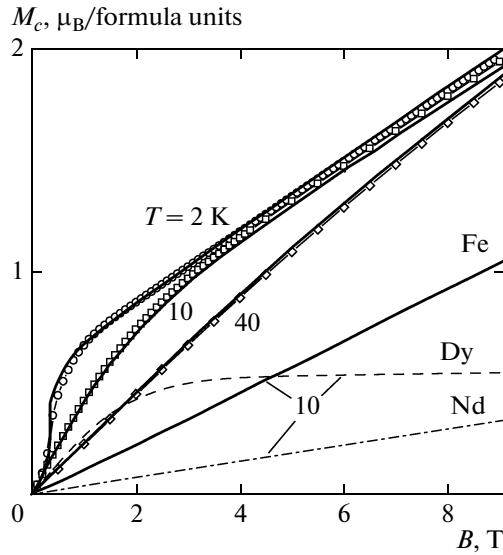


**Fig. 3.** Magnetization curves of  $\text{Nd}_{0.95}\text{Dy}_{0.05}\text{Fe}_3(\text{BO}_3)_4$  for  $\mathbf{B} \parallel \mathbf{c}$  at the given temperatures: (symbols) experimental data and (curves) calculation. Calculated contributions of the Nd, Dy, and Fe subsystems to the total magnetization at  $T = 10$  K are shown.

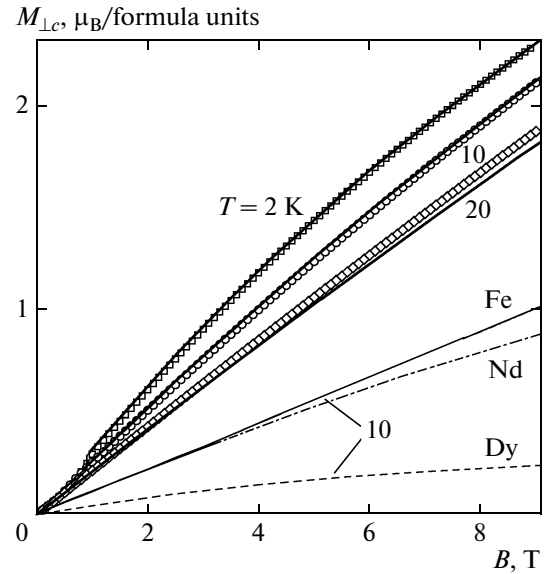


**Fig. 4.** Magnetization curves of  $\text{Nd}_{0.95}\text{Dy}_{0.05}\text{Fe}_3(\text{BO}_3)_4$  for  $\mathbf{B} \perp \mathbf{c}$  at the given temperatures: (symbols) experimental data and (curves) calculation. Calculated contributions of the Nd, Dy, and Fe subsystems to the total magnetization at  $T = 10$  K are shown.

tion of  $\text{Dy}^{3+}$  for  $\text{Nd}^{3+}$  ions. However, the magnetization curves of  $\text{NdFe}_3(\text{BO}_3)_4$  exhibit anomalies only during magnetization in the basal plane  $M_{a,b}(B)$  (near 0.7–0.8 T) and have no anomalies during magnetization along axis  $c$  [17, 29].

Thus, the analysis of the experimental data and the calculations performed on the assumption of an easy-axis or an easy-plane state in  $\text{Nd}_{0.95}\text{Dy}_{0.05}\text{Fe}_3(\text{BO}_3)_4$  at low temperatures and  $B = 0$  cannot explain the existence of anomalies in low fields in both magnetization curves, i.e.,  $M_c(B)$  and  $M_{\perp c}(B)$ .

In [12], we assumed the presence of a low-temperature magnetic state with the formation of a weakly noncollinear antiferromagnetic phase having the magnetic moments of iron deviating from axis  $c$  in order to explain the interesting steplike anomalies in the  $M_c(B)$  magnetization curves and the  $\chi_c(T)$  susceptibility curves of  $\text{Nd}_{1-x}\text{Dy}_x\text{Fe}_3(\text{BO}_3)_4$  ( $x = 0.15, 0.25$ ). As a result, we were able to achieve agreement between the calculated and experimental data for the entire set of measured characteristics of  $\text{Nd}_{1-x}\text{Dy}_x\text{Fe}_3(\text{BO}_3)_4$  using the same set of parameters [12]. Note that, when studying  $\text{GdFe}_3(\text{BO}_3)_4$  undergoing a spin-reorientation transition, the authors of [30] concluded that the magnetic moments of iron deviate from axis  $c$  through high angles, which change at various temperatures and magnetic fields (see, e.g., Fig. 6 in [30]).

Our extensive calculations of the magnetic phases that appear in  $\text{Nd}_{0.95}\text{Dy}_{0.05}\text{Fe}_3(\text{BO}_3)_4$  at various orientations of the magnetic moments of the Nd, Dy, and Fe subsystems suggest the presence of a low-temperature state that differs from both the easy-plane and the

easy-axis states. An antiferromagnetic phase with the magnetic moments of iron deviating from axis  $c$  through an angle  $\theta \approx 77^\circ$  (at  $T = 2$  K) appears; as a result, a cone of easy magnetization axes forms at  $B = 0$  (see Fig. 1c). This possible state can be caused by the competition between the contributions of the iron and rare-earth subsystems to the total magnetic anisotropy of  $\text{Nd}_{0.95}\text{Dy}_{0.05}\text{Fe}_3(\text{BO}_3)_4$ . The magnetic anisotropy of the neodymium subsystem stabilizes the easy-plane magnetic structure, the contribution of the dysprosium subsystem to the total anisotropy stabilizes the easy-axis structure, and the contribution of the iron subsystem (see Eq. (6)) with the found anisotropy constants is close to the easy-plane state. As a result, at certain temperatures and fields, the magnetic moments of iron can be oriented at angle  $\theta$  to axis  $c$ , which decreases when the temperature decreases from  $T \approx 4.3$  K and tends toward  $\theta = 77^\circ$  (see below).

Note that additional calculations demonstrate that the magnetic properties of  $\text{Nd}_{1-x}\text{Dy}_x\text{Fe}_3(\text{BO}_3)_4$  ferrobates for small substitution ( $x = 0.1, 0.15$ ) that were measured in [12, 13] can be described if the ground state at  $B = 0$  is represented by not the easy-axis state and the cone of easy magnetization axes has a low angle of deflection ( $\theta \approx 5^\circ\text{--}10^\circ$ ). It is expected that the new values of the  $f$ – $d$  exchange fields  $B_{fd}$  for  $x = 0.1$  and  $0.15$  are substantially closer to the values of  $B_{fd}$  in  $\text{NdFe}_3(\text{BO}_3)_4$  and  $\text{DyFe}_3(\text{BO}_3)_4$ , as for the composition with  $x = 0.05$  (see Table 2).

Further calculations demonstrate that the detected low-field anomalies in the experimental  $M_{c,\perp c}(B)$  magnetization curves at  $T = 2$  K and  $B < 1.5$  T (see

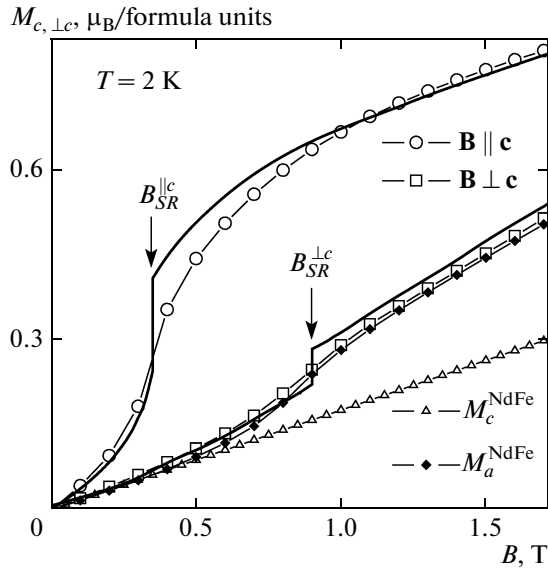


**Fig. 5.** Low-field region of the  $M_{c, \perp c}(B)$  magnetization curves of  $\text{Nd}_{0.95}\text{Dy}_{0.05}\text{Fe}_3(\text{BO}_3)_4$  for  $\mathbf{B} \parallel \mathbf{c}$  and  $\mathbf{B} \perp \mathbf{c}$  at  $T = 2$  K: (symbols) experimental data and (curves) calculation.  $M_{c, a}^{\text{NdFe}}(B)$  are the experimental magnetization curves of  $\text{NdFe}_3(\text{BO}_3)_4$  [29].

Fig. 5) are caused by the spin-reorientation transitions in the iron subsystem of  $\text{Nd}_{0.95}\text{Dy}_{0.05}\text{Fe}_3(\text{BO}_3)_4$  from the initial state at an angle to axis  $c$  (Figs. 1d, 1e) to the flop state (Figs. 1a, 1b).

We now dwell on the situation that appears during the magnetization of  $\text{Nd}_{0.95}\text{Dy}_{0.05}\text{Fe}_3(\text{BO}_3)_4$  in fields  $B < 1.5$  T, which are important from a standpoint of the detected anomalies. The magnetization jump in the experimental  $M_c(B)$  curve in a field  $B_{SR} \approx 0.35$  T in Fig. 5 is caused by the field-induced ( $\mathbf{B} \parallel \mathbf{c}$ ) spin-reorientation transition in the Fe subsystem of  $\text{Nd}_{0.95}\text{Dy}_{0.05}\text{Fe}_3(\text{BO}_3)_4$  from the initial weakly collinear phase (Fig. 1d) into the flop phase (Fig. 1a) and is accompanied by the reorientation of the magnetic moments of both sublattices of  $\text{Nd}^{3+}$  and  $\text{Dy}^{3+}$  ions along the field direction  $\mathbf{B} \parallel \mathbf{c}$ . It is seen that the resulting magnetizations in the initial phase,

$$M_c = \frac{1}{2}(M_1^{\text{Fe}} \cos(\vartheta_1) + M_2^{\text{Fe}} \cos(\vartheta_2)) + (1-x)m_{1,2c}^{\text{Nd}} + xm_{1,2c}^{\text{Dy}},$$

and in the flop phase (see Figs. 2, 5),

$$M_{\text{flop}} = \frac{1}{2}(M_{1,2c}^{\text{Fe}} + (1-x)m_{1,2c}^{\text{Nd}} + xm_{1,2c}^{\text{Dy}}),$$

well describe the experimental data. Our calculations show that the difference between  $M_c$  and  $M_{\text{flop}}$  in a field  $B_{SR} \approx 0.35$  T is mainly caused by a change in the contributions of the Dy and Fe subsystems to the magnetization of  $\text{Nd}_{0.95}\text{Dy}_{0.05}\text{Fe}_3(\text{BO}_3)_4$ .

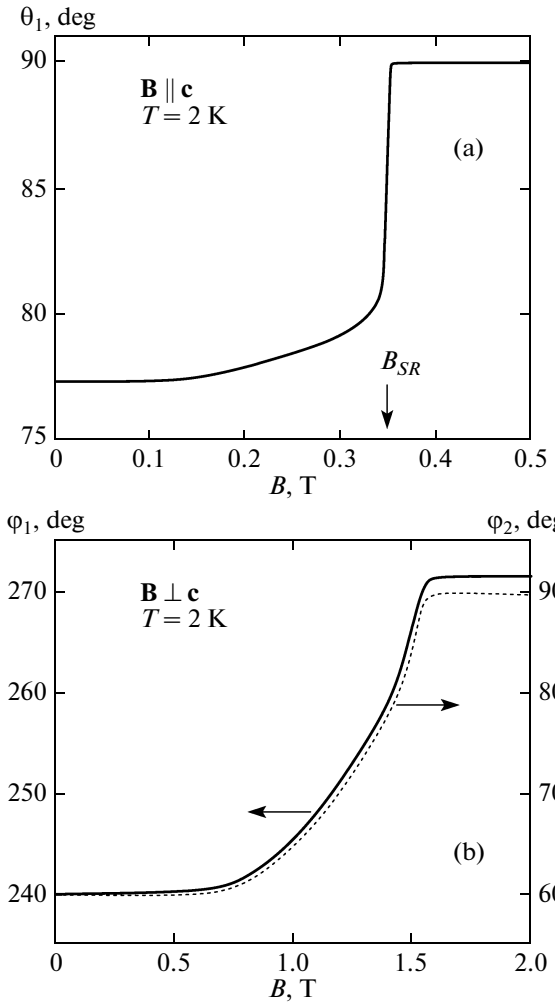


**Fig. 6.** Calculated (at  $T = 2$  K) field dependences of (a) angle of deviation  $\vartheta_1$  of magnetic moment  $\mathbf{M}_1^{\text{Fe}}$  from axis  $c$  for  $\mathbf{B} \parallel \mathbf{c}$  and (b) angles of deviation  $\varphi_{1,2}$  of magnetic moments  $\mathbf{M}_{1,2}^{\text{Fe}}$  in domains  $L_{60}$  from axis  $a$  in plane  $ab$  for  $\mathbf{B} \perp \mathbf{c}$  ( $\varphi_1 = 240^\circ$  for  $\mathbf{M}_1^{\text{Fe}}$ ,  $\varphi_2 = 60^\circ$  for  $\mathbf{M}_2^{\text{Fe}}$ ; see Fig. 1e).

As is seen from the calculated field dependence of the angle of rotation  $\vartheta_1$  of vector  $\mathbf{M}_1^{\text{Fe}}$  from trigonal axis  $c$  for  $\mathbf{B} \parallel \mathbf{c}$  (Fig. 6a), vector  $\mathbf{M}_1^{\text{Fe}}$  tends to rotate into plane  $ab$  normal to the field direction as the field grows. As the field  $B_{SR} \approx 0.35$  T is approached, the rate of increase of angle  $\vartheta_1$  increases and changes jumpwise to almost  $90^\circ$  at  $B_{SR}$ . Then, as the field grows, the magnetic moments of the Fe sublattices  $\mathbf{M}_1^{\text{Fe}}$  and  $\mathbf{M}_2^{\text{Fe}}$  bend slowly toward the field direction  $\mathbf{B} \parallel \mathbf{c}$ . The spin-flip transition is estimated to take place near 120 T.

Table 3 gives the magnetic moments of the Nd, Dy, and Fe subsystems in the phases under study for  $\mathbf{B} \parallel \mathbf{c}$  and  $T = 2$  K. The second column contains the mag-

**Table 3.** Magnetic moments of the Nd, Dy, and Fe subsystems at  $T = 2$  K ( $\mathbf{B} \parallel \mathbf{c}$ ,  $\varphi_1^{\text{Fe}} = 0$ ,  $\varphi_2^{\text{Fe}} = 180^\circ$ ):  $B = 0$  (initial antiferromagnetic phase at an angle to axis  $c$ ),  $B = 0.3$  T  $< B_{SR}$  (weakly noncollinear antiferromagnetic phase at an angle to axis  $c$ ), and  $B = 0.4$  and 9 T  $> B_{SR}$  (flop phase)

$m_i^R, M_i^{\text{Fe}}$	$B = 0$	$B = 0.3$ T	$B = 0.4$ T	$B = 9$ T
	$m_i^R(a, b, c), \mu_B$			
$m_1^{\text{Nd}_{0.95}}$	(-1.409, -0.01, -0.094)	(-1.414, -0.01, -0.064)	(-1.419, 0.002, 0.019)	(-1.32, 0.03, 0.4)
$m_2^{\text{Nd}_{0.95}}$	(1.409, 0.01, 0.094)	(1.411, 0.01, 0.0932)	(1.419, 0.002, 0.019)	(1.32, 0.03, 0.4)
$m_1^{\text{Dy}_{0.05}}$	(-0.143, -0.001, -0.48)	(-0.15, -0.001, -0.272)	(-0.149, 0.001, 0.395)	(-0.11, 0.001, 0.548)
$m_2^{\text{Dy}_{0.05}}$	(0.143, 0.001, 0.48)	(0.14, 0.001, 0.510)	(0.149, 0.001, 0.395)	(0.11, 0.001, 0.548)
$M_1^{\text{Fe}}$	$\vartheta_1, M_{1c}^{\text{Fe}} = M_1^{\text{Fe}} \cos \vartheta_1 (M_1^{\text{Fe}} = 15\mu_B, \varphi_1^{\text{Fe}} = 0)$			
	77.381°, 3.277 $\mu_B$	79.261°, 2.795 $\mu_B$	89.86°, 0.037 $\mu_B$	86.04°, 1.036 $\mu_B$
$M_2^{\text{Fe}}$	$\vartheta_2, M_{2c}^{\text{Fe}} = M_2^{\text{Fe}} \cos \vartheta_2 (M_2^{\text{Fe}} = 15\mu_B, \varphi_2^{\text{Fe}} = 180^\circ)$			
	102.619°, -3.277 $\mu_B$ (180° - $\vartheta_2$ - $\vartheta_1 = 0$ )	100.507°, -2.735 $\mu_B$ (180° - $\vartheta_2$ - $\vartheta_1 = 0.232^\circ$ )	89.86°, 0.037 $\mu_B$	86.04°, 1.036 $\mu_B$
$M_c$	$M_c = 0.5(M_{1c}^{\text{Fe}} + M_{2c}^{\text{Fe}} + m_{1c}^{\text{Nd}_{0.95}} + m_{2c}^{\text{Nd}_{0.95}} + m_{1c}^{\text{Dy}_{0.05}} + m_{2c}^{\text{Dy}_{0.05}})$			
	0	0.163	0.451	1.985

netic moments for  $B = 0$  in the initial antiferromagnetic phase at an angle to axis  $c$  (Fig. 1c, cone of easy magnetization axes). The third column presents the magnetic moments in the weakly collinear antiferromagnetic phase at an angle to axis  $c$  for  $B = 0.3$  T  $< B_{SR}$  (Fig. 1d). The two last columns give the magnetic moments in the flop phase at  $B > B_{SR}$  (Fig. 1a).

As is seen from Table 3, the magnetic moments of the Nd subsystem almost fully lie in the basal plane ( $|m_{1,2a}^{\text{Nd}_{0.95}}| \gg |m_{1,2c}^{\text{Nd}_{0.95}}|$ ), which explains their small contribution to the magnetization of the compound for  $\mathbf{B} \parallel \mathbf{c}$ , in particular, to the magnetization jump in the  $M_c(B)$  curve at  $B_{SR} \approx 0.35$  T. In this case, the Dy subsystem in the flop phase ( $B > B_{SR}$ ) is characterized by the magnetic moments of both sublattices directed mainly along the field ( $|m_{1,2c}^{\text{Dy}_{0.05}}| > |m_{1,2a}^{\text{Dy}_{0.05}}|$ ), which makes the main contribution to the magnetization jump during the spin-reorientation transition.

A trigonal crystal with magnetic moments lying in the basal plane can contain three types of antiferromagnetic domains, antiferromagnetism vector  $\mathbf{L}$  in each of which is oriented along the corresponding twofold axis. During the magnetization of a trigonal  $\text{Nd}_{0.95}\text{Dy}_{0.05}\text{Fe}_3(\text{BO}_3)_4$  crystal in the basal plane in fields lower than 1.5 T, all three possible domains with antiferromagnetism axes located at an angle of  $120^\circ$  to

each other contribute to the magnetization. The  $M_{\perp c}(B)$  magnetization curves for  $B < 1.5$  T were calculated using the approach proposed in [17], where the magnetization processes in easy-plane  $\text{NdFe}_3(\text{BO}_3)_4$  were comprehensively studied with allowance for the possible existence of domains of the tree types. Since information on the domain structure of the sample was absent, the domain sizes were assumed to be the same.

During magnetization in the basal plane for  $\mathbf{B} \parallel \mathbf{a}$ , the magnetic moments of iron in a domain with the antiferromagnetism axis along the field  $L_0$  ( $L_{0ab}$  is the projection onto plane  $ab$ ; Figs. 1c, 1e) make a contribution increasing with the field due to an increase in bending toward field  $\mathbf{B} \parallel \mathbf{a}$ . Magnetic moment  $\mathbf{m}_{1ab}$  directed opposite to the field in the rare-earth subsystem decreases. As a result, the total magnetization of domain  $L_0$  increases weakly with the field and repeats the character of the experimental  $M_{\perp c}(B)$  dependence. Both magnetic moments of iron  $\mathbf{M}_{1,2ab}^{\text{Fe}}$  in two other domains  $L_{60ab}$  with antiferromagnetism axes located at an angle of  $\varphi = 60^\circ$  to the field (which are equivalent with respect to field direction  $\mathbf{B} \parallel \mathbf{a}$ ) rotate toward the flop state (Fig. 1e). It is seen from the calculated field dependence of the angles of rotation  $\varphi_{1,2}$  of the  $\mathbf{M}_{1,2ab}^{\text{Fe}}$  vectors in domain  $L_{60}$  in plane  $ab$  that vector  $\mathbf{M}_{1ab}^{\text{Fe}}$  rotates slightly faster than  $\mathbf{M}_{2ab}^{\text{Fe}}$  does

(Fig. 6b). The contribution of domain  $L_{60ab}$  to the magnetization increases because of different rates of rotation of the  $\mathbf{M}_{1,2ab}^{\text{Fe}}$  vectors. The total magnetization for field  $\mathbf{B} \parallel \mathbf{a}$  and  $B < B_{SR}$ ,

$$M_a = \frac{1}{2} \left[ \frac{1}{3} (M_0^{\text{Fe}} + (1-x)m_{1,2a}^{\text{Nd}} + xm_{1,2a}^{\text{Dy}}) + \frac{2}{3} (M_{60}^{\text{Fe}} + (1-x)m_{1,2a}^{\text{Nd}} + xm_{1,2a}^{\text{Dy}}) \right] \quad (11)$$

well describes the experimental  $M_{\perp c}(B)$  curve (see Fig. 5). In Eq. (11),  $M_0^{\text{Fe}} = M_1^{\text{Fe}} \sin(\vartheta_1) - M_2^{\text{Fe}} \sin(\vartheta_2)$  is the contribution of iron to the magnetization of domain  $L_{0ab}$  with allowance for the projection onto plane  $ab$ , and  $M_{60}^{\text{Fe}} = M_1^{\text{Fe}} \sin(\vartheta_1) \cos(\varphi_1) + M_2^{\text{Fe}} \sin(\vartheta_2) \cos(\varphi_2)$  is the contribution of iron to the magnetization of domain  $L_{60ab}$  with allowance for the projection onto plane  $ab$  and axis  $a$ .

In a field  $B_{SR} \approx 0.9$  T, a spin-reorientation transition into the flop state with magnetic moments almost perpendicular to the field takes place in domain  $L_0$ , and its magnetization with allowance for the projection onto plane  $ab$  is  $M_{\text{flop}}^{\text{Fe}} = 2M_1^{\text{Fe}} \sin(\vartheta_1) \cos(\varphi_1)$  (see Fig. 1b). As a result, the total magnetization for  $B > B_{SR}$  is

$$M_a = \frac{1}{2} \left[ \frac{1}{3} (M_{\text{flop}}^{\text{Fe}} + (1-x)m_{1,2a}^{\text{Nd}} + xm_{1,2a}^{\text{Dy}}) + \frac{2}{3} (M_{60}^{\text{Fe}} + (1-x)m_{1,2a}^{\text{Nd}} + xm_{1,2a}^{\text{Dy}}) \right]. \quad (12)$$

As the field increases further, magnetic moments  $\mathbf{M}_{1,2ab}^{\text{Fe}}$  continue to rotate in domains  $L_{60ab}$ , and calculations show that the rate of rotation increases with the field. Beginning from a field of about 1.5 T, the total magnetization differs weakly from the magnetization in the flop phase.

It is seen from Figs. 5 and 2 that the calculated magnetization curves, which are characterized by magnetization jumps, can describe the experimental curves if we take into account that these jumps in a real sample should be smeared because of the presence of a domain structure. Note that the rotation and jumps of the magnetic moments of iron in all domains are accompanied by changes in the components of the magnetic moments in the rare-earth subsystem. The spin-reorientation transition fields in the calculations were determined from the equality of the thermodynamic potentials of the corresponding magnetic phases.

Taking into account the large contribution of the Nd subsystem to Nd<sub>0.95</sub>Dy<sub>0.05</sub>Fe<sub>3</sub>(BO<sub>3</sub>)<sub>4</sub> and the possible existence of easy-plane [2, 17, 31] and spiral [32, 33] magnetic structures in NdFe<sub>3</sub>(BO<sub>3</sub>)<sub>4</sub>, we cannot exclude that such a spiral structure forms in

Nd<sub>0.95</sub>Dy<sub>0.05</sub>Fe<sub>3</sub>(BO<sub>3</sub>)<sub>4</sub> at low temperatures. Note that the character of the anomalies in the experimental magnetization curves in the basal plane in Nd<sub>0.95</sub>Dy<sub>0.05</sub>Fe<sub>3</sub>(BO<sub>3</sub>)<sub>4</sub> is similar to that in NdFe<sub>3</sub>(BO<sub>3</sub>)<sub>4</sub> [29] and other easy-plane ferrobates (YFe<sub>3</sub>(BO<sub>3</sub>)<sub>4</sub> [34], EuFe<sub>3</sub>(BO<sub>3</sub>)<sub>4</sub> [4], SmFe<sub>3</sub>(BO<sub>3</sub>)<sub>4</sub> [35]). Since the detected anomalies in the  $M_{\perp c}(B)$  curves are analogous for all easy-plane ferrobates and a spiral character of the magnetic structure is assumed only in NdFe<sub>3</sub>(BO<sub>3</sub>)<sub>4</sub>, we can suppose that the possible existence of a spiral structure in NdFe<sub>3</sub>(BO<sub>3</sub>)<sub>4</sub> and Nd<sub>0.95</sub>Dy<sub>0.05</sub>Fe<sub>3</sub>(BO<sub>3</sub>)<sub>4</sub> weakly affects the character of the anomalies in  $M_{\perp c}(B)$  due to, e.g., small anisotropy in plane  $ab$ . The achieved agreement between the calculated and experimental  $M_{\perp c}(B)$  curves for Nd<sub>0.95</sub>Dy<sub>0.05</sub>Fe<sub>3</sub>(BO<sub>3</sub>)<sub>4</sub> and other ferrobates (NdFe<sub>3</sub>(BO<sub>3</sub>)<sub>4</sub> [17], SmFe<sub>3</sub>(BO<sub>3</sub>)<sub>4</sub> [35]) supports the assumption about a weak effect of a spiral magnetic structure, at least on the magnetic characteristics.

Both the iron subsystem ordered at  $T < T_N$  and the rare-earth subsystem magnetized by the  $f-d$  interaction contribute to the initial magnetic susceptibility of Nd<sub>0.95</sub>Dy<sub>0.05</sub>Fe<sub>3</sub>(BO<sub>3</sub>)<sub>4</sub>. Figure 7 shows the experimental and calculated temperature dependences of magnetic susceptibility  $\chi_{c,\perp c}(T)$ . At  $T_N \approx 30$  K, the experimental curve exhibits a weak anomaly, which is caused by antiferromagnetic ordering in the Fe subsystem. The calculated Néel temperature is slightly higher than the experimental value, which is a well-known disadvantage of the molecular field approximation. The calculations demonstrate that the anisotropy of the  $\chi_{c,\perp c}(T)$  curves in the paramagnetic temperature range is mainly caused by the contribution of the dysprosium part of the rare-earth system. The detected significant increase in the  $\chi_c(T)$  curve at  $T < T_N$  is also related to the contribution of the Dy subsystem. On the whole, the susceptibility curves calculated in the high-temperature range from  $T_N \approx 30$  K to  $T \approx 300$  K well describe the weakly anisotropic  $\chi_{c,\perp c}(T)$  experimental curves.

The inset to Fig. 7 shows the low-temperature regions (for  $T < T_N$ ) of the experimental and calculated  $\chi_{c,\perp c}(T)$  dependences of Nd<sub>0.95</sub>Dy<sub>0.05</sub>Fe<sub>3</sub>(BO<sub>3</sub>)<sub>4</sub>. For comparison, the inset also depicts the experimental  $\chi_{c,b}^{\text{NdFe}}(T)$  curves of NdFe<sub>3</sub>(BO<sub>3</sub>)<sub>4</sub> [29]. When comparing the susceptibility curves for Nd<sub>0.95</sub>Dy<sub>0.05</sub>Fe<sub>3</sub>(BO<sub>3</sub>)<sub>4</sub> and easy-plane NdFe<sub>3</sub>(BO<sub>3</sub>)<sub>4</sub>, we can conclude that the small substitution of Dy<sup>3+</sup> for Nd<sup>3+</sup> ions only weakly affects the character of susceptibility in the basal plane: the  $\chi_{\perp c}(T)$  curve of Nd<sub>0.95</sub>Dy<sub>0.05</sub>Fe<sub>3</sub>(BO<sub>3</sub>)<sub>4</sub> repeats the shape of  $\chi_b^{\text{NdFe}}(T)$  of NdFe<sub>3</sub>(BO<sub>3</sub>)<sub>4</sub> (including the Schottky-type anomaly near 5.5 K) and lies slightly higher. However, the small substitution radically changes the shape of the  $\chi_c(T)$  curve of Nd<sub>0.95</sub>Dy<sub>0.05</sub>Fe<sub>3</sub>(BO<sub>3</sub>)<sub>4</sub>. It is seen that the additional contribution of the Dy<sub>0.05</sub> subsystem

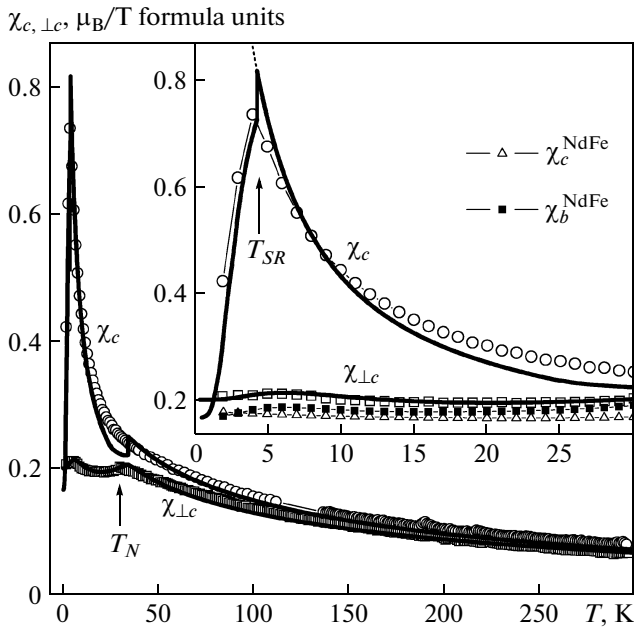


**Fig. 7.** Temperature dependences of the initial magnetic susceptibility  $\chi_{c,\perp c}(T)$  at  $B = 0.1$  T. For clarity, the temperature axis begins with  $-7$  K. (inset) Low-temperature region of the  $\chi_{c,\perp c}(T)$  and  $\chi_{c,b}^{\text{NdFe}}$  ( $T$ )  $\text{NdFe}_3(\text{BO}_3)_4$  [29] curves at  $T < T_N$ . (symbols) Experimental data and (curves) calculation.

leads to a significant quantitative change in susceptibility  $\chi_c(T)$  and to the pronounced anomaly at  $T \approx 4.3$  K, which is absent in  $\chi_c^{\text{NdFe}}(T)$ .

As the temperature decreases from  $T_N \approx 30$  K, the experimental  $\chi_c(T)$  curve continues to increase, which is characteristic of the easy-plane state of the magnetic subsystem. At  $T \approx 4.3$  K,  $\chi_c(T)$  decreases sharply, which can be explained by the presence of a spin-reorientation transition from the easy-plane state into the initial low-temperature state, the character and specific features of which in  $\text{Nd}_{0.95}\text{Dy}_{0.05}\text{Fe}_3(\text{BO}_3)_4$  are not obvious if only susceptibility  $\chi_c(T)$  is analyzed. Such behavior of susceptibility was earlier observed in  $\text{Nd}_{1-x}\text{Dy}_x\text{Fe}_3(\text{BO}_3)_4$  ( $x = 0.1$  [13],  $0.15$  [12],  $0.25$  [8, 12],  $0.4$  [14]) and was explained by a spin-reorientation transition from the easy-plane into the easy-axis state. However, magnetization curves for  $\text{Nd}_{1-x}\text{Dy}_x\text{Fe}_3(\text{BO}_3)_4$  ( $x = 0.1, 0.15, 0.25, 0.4$ ) exhibited anomalies only in the  $M_c(B)$  curve [12–14]. As discussed above, weakly substituted  $\text{Nd}_{0.95}\text{Dy}_{0.05}\text{Fe}_3(\text{BO}_3)_4$  exhibits low-field anomalies in both  $M_c(B)$  and  $M_{\perp c}(B)$ , which indicates a significant change in the contributions of the R and Fe subsystems to the magnetization in a low field for both  $\mathbf{B} \parallel \mathbf{c}$  and  $\mathbf{B} \perp \mathbf{c}$ .

The calculations demonstrate that the antiferromagnetic phase with the magnetic moments of iron deviating from axis  $c$  through an angle  $\theta \approx 77^\circ$  at  $T =$

2 K that was suggested during analysis of the low-field  $M_{c,\perp c}(B)$  magnetization curves can be used to explain and to quantitatively describe the anomaly detected experimentally in the  $\chi_c(T)$  curve near  $T = 4.3$  K (see Fig. 1c). The sharp decrease in  $\chi_c(T)$  at  $T = 4.3$  K is caused by the change from the easy-plane to the low-temperature state with the magnetic moments of iron deviating from axis  $c$  when the temperature decreases (see Fig. 1c). This spin-reorientation transition is caused by the different temperature dependences of the competing contributions of the iron and rare-earth subsystems to the total magnetic anisotropy of  $\text{Nd}_{0.95}\text{Dy}_{0.05}\text{Fe}_3(\text{BO}_3)_4$ .

The tendency toward the manifestation of an easy-plane character of the magnetic subsystem that was detected in  $\text{Nd}_{0.95}\text{Dy}_{0.05}\text{Fe}_3(\text{BO}_3)_4$  with increasing temperature agrees with the results obtained for  $\text{Nd}_{1-x}\text{Dy}_x\text{Fe}_3(\text{BO}_3)_4$  ( $x = 0.1-0.4$ ) [8, 12–14],  $\text{Sm}_{0.7}\text{Ho}_{0.3}\text{Fe}_3(\text{BO}_3)_4$  [15],  $\text{HoFe}_3(\text{BO}_3)_4$  [22, 36], and  $\text{Ho}_{0.5}\text{Nd}_{0.5}\text{Fe}_3(\text{BO}_3)_4$  [3], where an easy-plane magnetic structure formed when the temperature increased after the spin-reorientation transition. The dashed curve shown in the inset to Fig. 7 and calculated below  $T_{SR}$  demonstrates the further run of the  $\chi_c(T)$  curve in the easy-plane state for the case if the magnetic moments of the rare-earth and iron subsystems in  $\text{Nd}_{0.95}\text{Dy}_{0.05}\text{Fe}_3(\text{BO}_3)_4$  were not reoriented at  $T_{SR} \approx 4.3$  K.

During magnetization in the basal plane for  $B = 0.1$  T, all possible domains contribute to susceptibility  $\chi_{\perp c}(T)$  and the magnetization processes in  $\text{Nd}_{0.95}\text{Dy}_{0.05}\text{Fe}_3(\text{BO}_3)_4$  occur similarly to those described in [17] for easy-plane  $\text{NdFe}_3(\text{BO}_3)_4$ . For  $\mathbf{B} \perp \mathbf{c}$ , the temperature dependence of susceptibility  $\chi_{\perp c}(T)$  near  $T = 5.5$  K demonstrates a Schottky-type anomaly, which is caused by the redistribution of the population of the lower levels of the  $\text{Nd}^{3+}$  ion and is well reproduced by calculations.

## CONCLUSIONS

The magnetic properties of the weakly substituted  $\text{Nd}_{0.95}\text{Dy}_{0.05}\text{Fe}_3(\text{BO}_3)_4$  ferroborate with competing Nd–Fe and Dy–Fe exchange interactions were studied experimentally and theoretically, and agreement between the calculated and experimental data was achieved for the entire set of measured characteristics. Using a general theoretical approach based on the crystal field model for a rare-earth ion and the molecular field approximation, we were able to determine the parameters of  $\text{Nd}_{0.95}\text{Dy}_{0.05}\text{Fe}_3(\text{BO}_3)_4$  by comparing the calculated and experimental results. The found parameters were presented in a table for the entire family of  $\text{Nd}_{1-x}\text{Dy}_x\text{Fe}_3(\text{BO}_3)_4$  ( $x = 0.05, 0.1, 0.15, 0.25, 0.4$ ) ferroborates studied using the proposed approach. The effect of small substitution of  $\text{Dy}^{3+}$  for  $\text{Nd}^{3+}$  ions on the magnetic properties of  $\text{Nd}_{0.95}\text{Dy}_{0.05}\text{Fe}_3(\text{BO}_3)_4$  was analyzed, and the degrees

of responsibility of the contribution of each subsystem for the detected effects were found.

The proposed version of the magnetization processes in Nd<sub>0.95</sub>Dy<sub>0.05</sub>Fe<sub>3</sub>(BO<sub>3</sub>)<sub>4</sub> in low magnetic fields with the formation of an antiferromagnetic state with the magnetic moments of iron deviating from axis *c* through angle  $\theta$  ( $\theta \approx 77^\circ$  at  $T = 2$  K and  $B = 0$ ) made it possible to comprehensively analyze the behavior of the magnetic moments of the R and Fe subsystems and to describe the nonlinear low-temperature  $M_{c,\perp c}(B)$  magnetization curves, which indicated phase transitions from the initial phase into a flop phase. For Nd<sub>0.95</sub>Dy<sub>0.05</sub>Fe<sub>3</sub>(BO<sub>3</sub>)<sub>4</sub>, we detected and described a spontaneous spin-reorientation transition near  $T_{SR} \approx 4.3$  K, which manifested itself as a pronounced anomaly in the susceptibility curve  $\chi_c(T)$ . We used one set of parameters and anisotropy constants  $K_{2,4,66}^{\text{Fe}}$  and used no adjustable parameters to calculate the  $\chi_{c,\perp c}(T)$  susceptibility curves in the ordered and paramagnetic temperature ranges and to calculate the field dependences of the  $M_{c,\perp c}(B)$  magnetization curves up to 9 T.

#### ACKNOWLEDGMENTS

This work was supported by the Russian Foundation for Basic Research (project no. 12-02-31007mol\_a) and the President of the Russian Federation (grant no. MK-1700.2013.2).

#### REFERENCES

1. A. K. Zvezdin, S. S. Krotov, A. M. Kadomtseva, G. P. Vorob'ev, Yu. F. Popov, A. P. Pyatakov, L. N. Bezmaternykh, and E. A. Popova, JETP Lett. **81** (6), 272 (2005).
2. A. K. Zvezdin, G. P. Vorob'ev, A. M. Kadomtseva, Yu. F. Popov, A. P. Pyatakov, L. N. Bezmaternykh, A. V. Kuvardin, and E. A. Popova, JETP Lett. **83** (11), 509 (2006).
3. R. P. Chaudhury, F. Yen, B. Lorenz, Y. Y. Sun, L. N. Bezmaternykh, V. L. Temerov, and C. W. Chu, Phys. Rev. B: Condens. Matter **80**, 104424 (2009).
4. A. M. Kadomtseva, Yu. F. Popov, G. P. Vorob'ev, A. P. Pyatakov, S. S. Krotov, K. I. Kamilov, V. Yu. Ivanov, A. A. Mukhin, A. K. Zvezdin, A. M. Kuz'menko, L. N. Bezmaternykh, I. A. Gudim, and V. L. Temerov, Low Temp. Phys. **36** (6), 511 (2010).
5. Yu. F. Popov, A. P. Pyatakov, A. M. Kadomtseva, G. P. Vorob'ev, A. K. Zvezdin, A. A. Mukhin, V. Yu. Ivanov, and I. A. Gudim, JETP **111** (2), 199 (2010).
6. A. A. Mukhin, G. P. Vorob'ev, V. Yu. Ivanov, A. M. Kadomtseva, A. S. Narizhnaya, A. M. Kuz'menko, Yu. F. Popov, L. N. Bezmaternykh, and I. A. Gudim, JETP Lett. **93** (5), 275 (2011).
7. A. M. Kadomtseva, G. P. Vorob'ev, Yu. F. Popov, A. P. Pyatakov, A. A. Mukhin, V. Yu. Ivanov, A. K. Zvezdin, I. A. Gudim, V. L. Temerov, and L. N. Bezmaternykh, JETP **114** (5), 810 (2012).
8. Yu. F. Popov, A. M. Kadomtseva, G. P. Vorob'ev, A. A. Mukhin, V. Yu. Ivanov, A. M. Kuz'menko, A. S. Prokhorov, L. N. Bezmaternykh, and V. L. Temerov, JETP Lett. **89** (7), 345 (2009).
9. A. K. Zvezdin, A. M. Kadomtseva, Yu. F. Popov, G. P. Vorob'ev, A. P. Pyatakov, V. Yu. Ivanov, A. M. Kuz'menko, A. A. Mukhin, L. N. Bezmaternykh, and I. A. Gudim, JETP **109** (1), 68 (2009).
10. G. A. Zvyagina, K. R. Zhekov, I. V. Bilych, A. A. Zvyagin, L. N. Bezmaternykh, and I. A. Gudim, Low Temp. Phys. **36** (4), 296 (2010).
11. A. V. Malakhovskii, E. V. Eremin, and D. A. Velikanov, A. V. Kartashev, A. D. Vasil'ev, and I. A. Gudim, Phys. Solid State **53** (10), 2032 (2011).
12. A. A. Demidov, I. A. Gudim, and E. V. Eremin, JETP **114** (2), 259 (2012).
13. A. A. Demidov, I. A. Gudim, and E. V. Eremin, Physica B (Amsterdam) **407**, 393 (2012).
14. A. A. Demidov, I. A. Gudim, and E. V. Eremin, Solid State Phenom. **190**, 261 (2012).
15. A. A. Demidov, I. A. Gudim, and E. V. Eremin, JETP **115** (5), 815 (2012).
16. G. A. Zvyagina, K. R. Zhekov, A. A. Zvyagin, I. A. Gudim, and I. V. Bilych, Low Temp. Phys. **38** (5), 446 (2012).
17. D. V. Volkov, A. A. Demidov, and N. P. Kolmakova, JETP **104** (6), 897 (2007).
18. D. V. Volkov, A. A. Demidov, and N. P. Kolmakova, JETP **106** (4), 723 (2008).
19. I. A. Gudim, E. V. Eremin, and V. L. Temerov, J. Cryst. Growth **312**, 2427 (2010).
20. E. A. Popova, D. V. Volkov, A. N. Vasiliev, A. A. Demidov, N. P. Kolmakova, I. A. Gudim, L. N. Bezmaternykh, N. Tristan, Yu. Skourski, B. Büchner, C. Hess, and R. Klingeler, Phys. Rev. B: Condens. Matter **75**, 224413 (2007).
21. A. A. Demidov, N. P. Kolmakova, D. V. Volkov, and A. N. Vasiliev, Physica B (Amsterdam) **404**, 213 (2009).
22. A. A. Demidov and D. V. Volkov, Phys. Solid State **53** (5), 985 (2011).
23. A. A. Demidov and D. V. Volkov, Phys. Solid State **54** (3), 537 (2012).
24. Y. Hinatsu, Y. Doi, K. Ito, M. Wakeshima, and A. Alemi, J. Solid State Chem. **172**, 438 (2003).
25. E. P. Chukalina, D. Yu. Kuritsin, M. N. Popova, M. N. Popova, L. N. Bezmaternykh, S. A. Kharlamova, and V. L. Temerov, Phys. Lett. A **322**, 239 (2004).
26. A. K. Zvezdin, V. M. Matveev, A. A. Mukhin, and A. I. Popov, *Rare-Earth Ions in Magnetically Ordered Crystals* (Nauka, Moscow, 1985) [in Russian].
27. I. E. Dzyaloshinskii, Sov. Phys. JETP **5**, 1259 (1957).
28. A. I. Pankrats, G. A. Petrakovskii, L. N. Bezmaternykh, and V. L. Temerov, Phys. Solid State **50** (1), 79 (2008).
29. E. A. Popova, N. Tristan, C. Hess, R. Klingeler, B. Büchner, L. N. Bezmaternykh, V. L. Temerov, and A. N. Vasil'ev, JETP **105** (1), 105 (2007).
30. S. A. Kharlamova, S. G. Ovchinnikov, A. D. Balaev, M. F. Thomas, I. S. Lyubutin, and A. G. Gavriluk, JETP **101** (6), 1098 (2005).

31. J. E. Hamann-Borrero, M. Philipp, O. Kataeva, M. V. Zimmermann, J. Geck, R. Klingeler, A. Vasiliev, L. Bezmaternykh, B. Büchner, and C. Hess, *Phys. Rev. B: Condens. Matter* **82**, 094411 (2010).
32. P. Fischer, V. Pomjakushin, D. Sheptyakov, L. Keller, M. Janoschek, B. Roessli, J. Schefer, G. Petrakovskii, L. Bezmaternikh, V. Temerov, and D. Velikanov, *J. Phys.: Condens. Matter* **18**, 7975 (2006).
33. M. Janoschek, P. Fischer, J. Schefer, B. Roessli, V. Pomjakushin, M. Meven, V. Petricek, G. Petrakovskii, and L. Bezmaternikh, *Phys. Rev. B: Condens. Matter* **81**, 094429 (2010).
34. E. A. Popova, A. N. Vasiliev, V. L. Temerov, L. N. Bezmaternykh, N. Tristan, R. Klingeler, and B. Büchner, *J. Phys.: Condens. Matter* **22**, 116006 (2010).
35. A. A. Demidov, D. V. Volkov, I. A. Gudim, E. V. Eremin, and V. L. Temerov, *JETP* **116** (5), 800 (2013).
36. C. Ritter, A. Vorotynov, A. Pankrats, G. Petrakovskii, V. Temerov, I. Gudim, and R. Szymczak, *J. Phys.: Condens. Matter* **20**, 365209 (2008).

*Translated by K. Shakhlevich*